Abstract

We perform a numerical analysis of the propagation of electromagnetic waves that originate below the Earth's surface and are observed at low Earth orbit (LEO) altitudes, in support of recent missions such as QuakeSat I and Demeter, whose primary objective is the detection and identification of seismogenic electromagnetic signals. For our investigation we subdivide the intervening medium between source and observation into a large number of horizontally stratified, anisotropic slabs and solve the full-wave equations using the matrix method introduced by Nagano et al. [1975]. The effects of the altitude variations of the conducting ground, ionospheric electron density and collision frequency, as well as ion composition are easily included in our model, and we present results as a function of wave frequency and initial wave normal angle for the example case of the Dec. 22 2004, M6.4 San Simeon earthquake.

Full Wave Calculation of the Source Characteristics of Seismogenic Electromagnetic Signals as Observed at LEO Satellite Altitudes

J. Bortnik and T. Bleier

T51B-0453

Author Contact Information

Jacob Bortnik[1,2]: jbortnik@gmail.com
Thomas Bleier[1]: tbleier@quakefinder.com

Authors affiliations:
1. QuakeFinder, 250 Cambridge Avenue, Suite 204 , Palo Alto, CA 94306
2. Department of Atmospheric and Oceanic Sciences, UCLA
Room 7115, Mathematical Sciences Bldg. , Los Angeles, CA 90095

1. Introduction

Figure 1a: Examples Loma Prieta damage

Earthquakes are among the most destructive forces of nature, causing innumerable loss of lives and financial damage. For example, the 1989 Ms 7.1 Loma Prieta resulted in 62 deaths, 3000 injuries, and a minimum of $8.3 billion in direct damage.

Potential electromagnetic precursors

We show in Figure 1b a number of ULF signals recorded in Corralitos (located ~7km from the epicenter) before, during, and after the quake and reported by Fraser Smith et al. [1990] and Bernardi et al. [1991].

The recorded data shows the appearance of a tone in the 0.05-0.2Hz band beginning on Sept 12th (~5 weeks before quake), and a substantal increase in power in all bands starting Oct 5th (~2 weeks before quake). Followed by a sharp decrease on strength about one day before the quake was a dramatic increase to very levels in the 0.01-0.5 Hz band, approximately 3 hours before the earthquake. Given that there was no substantial ground shaking or geomagnetic activity, these measurements offer compelling evidence for a magnetic precursor.

Electromagnetic signals potentially linked to earthquakes have also been measured aboard satellites and reported in the literature [Serebryakova et al., 1992, Molchanov et al., 1993, Parrot 1994].

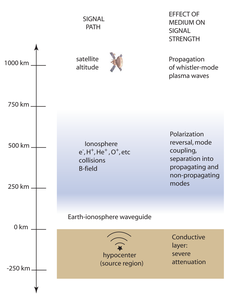

Figure 1d: Propagation characteristics of seismogenic electromagnetic waves

Aim of current work

We aim to support current missions such as Demeter and quakeSat I (Figure 1c) that have been deployed specifically in search of seismogenic electromagnetic signals, with theoretical work designed to understand the propagation of such signals from the lithosphere to the topside ionosphere.

Figure 1d shows a diagram of the signal path, showing the severe attenuation experienced in the conductive ground, reflection and transmission at the ground-air interface, attenuation, polarization reversal and mode coupling in the ionosphere as well as separation into a propagating and non-propagating mode.

Our modeling work will reproduce the features listed above, and provide bounds in parameter space (i.e., frequency, location) that will drive the search in current and future missions.

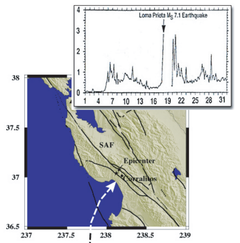

Figure 1b: Potential magnetic precursors to Loma Prieta earthquake

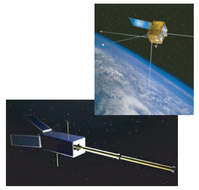

Figure 1c: Demeter (top) and QuakeSat I satellites

2. Modeling the wave propagation

Constituitive relations:

Since our solution space involves sharp gradients in refractive index, we resort to a "full-wave solution", i.e., solve Maxwell's equations in the presence of electrons and several ion species. Assume sinusoidal field excitation.

$$\nabla\times\vec{H}=\vec{J}+\frac{\partial\vec{D}}{\partial t}=j\omega\varepsilon_0\left(\vec{I}+\vec{M}\right)\vec{E}$$

$$\nabla\times\vec{E}=-\frac{\partial\vec{B}}{\partial t}=-j\omega\mu_0\vec{H}$$

$$\vec{J}=\sum_s N_s q_s\vec{v}_s$$

$$m_s\frac{d\vec{v}_s}{dt}=q_s\left(\vec{E}+\vec{v}\times\vec{B}\right)$$

Define direction vectors associated with the method geometry (Fig. 2a):

B-field	k-vector
$\gamma=\cos(\mathrm{DIP})$	$l=\sin(\mathrm{I})\sin(\chi)$
$\xi=-\sin(\mathrm{DIP})$	$m=\sin(\mathrm{I})\cos(\chi)$
	$q_l=\cos(\mathrm{I})$

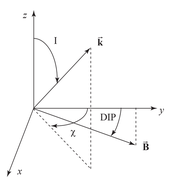

Figure 2a: method geometry

And the resultant susceptibility matrix M, becomes:

$$\vec{\vec{M}}=\begin{bmatrix}M_{xx}&M_{xy}&M_{xz}\\M_{yx}&M_{yy}&M_{yz}\\M_{zx}&M_{zy}&M_{zz}\end{bmatrix}=\begin{bmatrix}S-1&j\xi D&-j\gamma D\\-j\xi D&\xi^2S+\gamma^2P-1&\xi\gamma(P-S)\\j\gamma D&\xi\gamma(P-S)&\xi^2S+\gamma^2P-1\end{bmatrix}$$

Where: $P\equiv1-\sum_s\frac{\omega_{ps}^2}{\omega^2}$, $R\equiv1-\sum_s\frac{\omega_{ps}^2}{\omega(\omega+\Omega_s)}$, $L\equiv1-\sum_s\frac{\omega_{ps}^2}{\omega(\omega-\Omega_s)}$,

$S=(R+L)/2$, $D=(R-L)/2$ $\omega_{ps}=N_s q_s^2/\varepsilon_0 m_s$, $\Omega_s=q_s B_0/m_s$

Where q_s, m_s and N_s the mass, charge, and density of the particle of species "s", ω is the wave radial frequency, and ε_0, μ_0 are the electric permittivity and permeability of free space.

The effects of collisions are included by modifying the mass of the particle by the collision frequency, i.e.,

$$m_s=m_{s0}\left(1-\frac{\nu_c}{\omega}\right)$$

As shown in Fig. 2b, we assume the medium is horizontally stratified, such that there are no variations in the x or y directions, and the only remaining derivatives are in the z direction.

The equation to solve now becomes:

$$\frac{d\vec{e}}{dz}=-jk_0\vec{\vec{T}}\cdot\vec{e} \quad (1)$$

Where:

$$\vec{e}=\begin{bmatrix}E_x\\-E_y\\Z_0H_y\\Z_0H_x\end{bmatrix},\quad \vec{\vec{T}}=\begin{bmatrix}\frac{-lM_{zy}}{1+M_{zz}}&\frac{lM_{zy}}{1+M_{zz}}&\frac{lm}{1+M_{zz}}&1-\frac{l^2}{1+M_{zz}}\\\frac{mM_{zy}}{1+M_{zz}}&\frac{-mM_{zy}}{1+M_{zz}}&1-\frac{m^2}{1+M_{zz}}&\frac{ml}{1+M_{zz}}\\-M_{yx}-ml+\frac{M_{yz}M_{zy}}{1+M_{zz}}&1+M_{yy}-l^2+\frac{M_{yz}M_{zy}}{1+M_{zz}}&\frac{-mM_{yz}}{1+M_{zz}}&\frac{lM_{yz}}{1+M_{zz}}\\1+M_{xx}-m^2-\frac{M_{xz}M_{zy}}{1+M_{zz}}&\frac{M_{xz}M_{zy}}{1+M_{zz}}-M_{xy}-ml&\frac{mM_{xz}}{1+M_{zz}}&\frac{-lM_{xz}}{1+M_{zz}}\end{bmatrix}$$

To solve equation (1), we follow the procedure of Nagano et al. [1975]. First, the matrix T is evaluated at the mth layer (see Fig 2b), and the eigenvectors are found. The two eigenvectors corresponding to the upward propagating modes are found, and (1) is evaluated downwards to layer 1 using the above starting conditions to obtain the full solution.

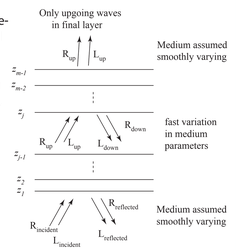

Figure 2b: Plane stratification and wave structure within medium

3. Simulation results

We apply the methodology described in Section 2, to the example earthquake of San Simeon, CA. which occurred on Dec. 22, 2003, 11:15am PST (35.706N 121.102W) Mw=6.5. First, medium parameters appropriate to the time and location of the quake are obtained, and then we examine the attenuation of electromagnetic signals as a function of frequency for vertical propagation in the earth, air, and in the entire earth-air path.

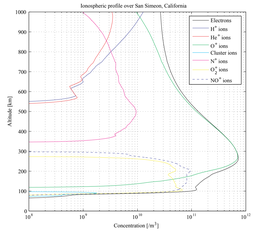

Figure 3a: Ionospheric density profile

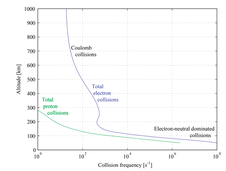

Figure 3b: Ionospheric collision-frequency profile

3.1 Medium parameters

To compute the P,R , L "Stix" parameters given in Section 2, we must specify the density and composition of the electron and ion populations as a function of altitude, as well as magnetic field intensity and dip angle. It is also necessary to know the collision profiles of electrons and ions since this critically controls attenuation and mode conversion.

To specify electron and ion number density we use the International Reference Ionosphere model [Bilitza, 1990] calculated at the geographic location of the quake at the approriate time. This profile is shown in Fig. 3a and indicates that the dominant ion species at altitudes of interest is Oxygen and the protonospheric transition occurs near ~950km.

The collision frequency was taken from Cummer [2000] for the low altitude portion of both electrons and protons (<300km), where collisions with neutrals are dominant. Above this altitude, Coulomb collisions dominate and we used the profile from Helliwell [1965, Fig 3-28].

The magnetic field intensity was calculated using IGRF, and assumed constant at 40μT, with DIP=60.3 degrees.

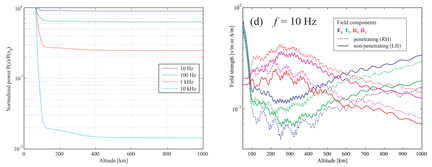

Figure 3c: Ionospheric power attenuation

3.2 Ionospheric propagation

To examine the behaviour of ELF electromagnetic waves propagating through the ionosphere, we show in Fig. 3d,e the wave components $|E_x|$, $|E_y|$, $|H_x|$, and $|H_y|$ associated with the 10 Hz and 100 Hz frequency components respectively. The plots show both propagating (RH) and non-propagating (LH) modes, and it is seen that at 10 Hz, both RH and LH modes are able to penetrate the ionosphere. At 100 Hz, the LH mode undergoes severe attenuation in the lower ionosphere, and only the RH mode penetrates. We also see the the 100 Hz wave experiences more attenuation in the D-region than the 10 Hz wave.

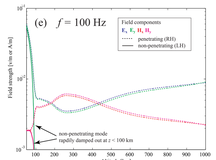

Figure 3d,e: $|E_x|$, $|E_y|$, $|H_x|$, $|H_y|$, versus altitude for (d) 10 Hz, and (e) 100 Hz.

To study wave power attenuation, we show in Fig. 3c the wave power, i.e., 1/2 Re(ExH) as a function of altitde for the propagating mode of various frequencies. As expected the higher frequencies experience more attenuation, but lower frequencies propagate almost entirely unaffected.

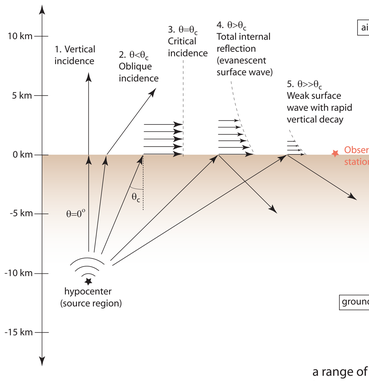

Figure 3k: Propagation of the electromagnetic wave from below ground to the surface, showing the critical angle, and evanescent wave with vertical attenuation.

3.3 Propagation in ground-ionosphere

We now combine the parameters of the ionosphere (Fig 3a,b) with the ground conductivity model (fig 3i - exponenetial conductivity profile) such the the susceptibility matrix M (Section 2) is specified at all points from below ground to above the ionosphere. The value of M below ground becomes:

$$M_{ij}=\begin{cases}\dfrac{-i\sigma}{\omega\varepsilon_0} & i=j\\ 0 & \text{otherwise}\end{cases}$$

where i,j = x,y,z.

As in Section 3.2, we show penetrating and non-penetrating modes in Fig 3f,g and note that in the ULF-ELF range both modes are able to traverse the ionosphere with only moderate losses.

The transmitted power - defined as the power at the topside ionosphere (1000 km) relative to the initial power - is plotted as a function of frequency from 0.01 Hz - 100 Hz in Fig 3h. We note that at frequencies below ~20 Hz, the non-penetrating mode crosses the ionosphere with losses comparable to the penetrating mode, but above this frequency is severely damped in the D-region (~60-90 km).

Overall, wave power attenuates only moderately for wave frequencies below ~10Hz, indicating that if such wave components were generated below ground, they might well penetrate the ionosphere and be observable aboard LEO satellites.

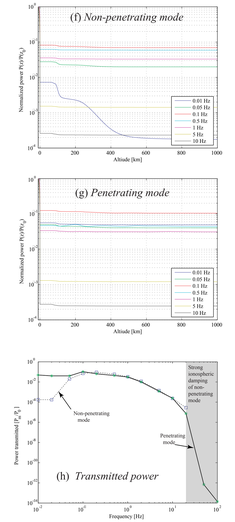

Figure 3f,g,h: Ground-ionosphere propagation; non-penetrating mode (f), penetrating mode (g), and transmitted power vs frequency (h).

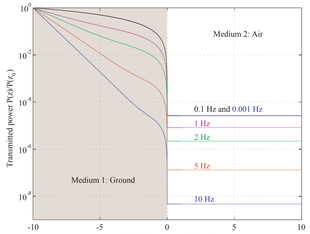

Figure 3j: Ground attenuation, reflection and transmission for various frequencies (constant conductivity model)

3.5 Ground propagation characteristics

We model the ground conductivity profile as shown in Fig 3i (constant conductivity) and use our full-wave model to calculate the transmitted power profiles for a range of frequencies as shown in Fig 3j. As expected, the attenuation increases as a function of frequency, however, on the low frequency end of the spectrum the skin depth (proportional to 1/sqrt(frequency)) becomes much larger than the ground propagation distance (skin depth of 10km occurs at f ~ 0.25 Hz), and is essentially unattenuated.

However, due to the extreme mismatch in the refractive indices of the ground and air, e.g., n_{ground}(1 Hz) = 10^4 (1+i), n_{air} = 1, the reflection coefficient is very close to unity and the transmitted wave is clamped at a low value (<10^{-4} in Fig. 3j). This indicates that lowering the observation frequency is not necessarily beneficial beyond a certain value and will not result in more power.

In contrast, the critical angle illustrated in Figure 3k above decreases sharply with decreasing frequency, and hence the region of observationabout the epicenter shrinks considerably. For the present case, the critical angle is ~0.007 degrees. While this small angle may at first seem prohibitive, it should be remembered that waves beyond the critical angle will still be observed above the surface as surface (or evanescent) waves which propagate horizontally and decay exponentially in altitude - the decay rate being dependent on the incident angle of the ray. The region about the epicenter where significant (observable) wave power exists will be the subject of future work with our model.

3.4 Ground conductivity model

To model the ground we use two different conductivity profiles as shown in Fig 3i. Typical resistivity values in the San Andreas Fault have recently been reported by Park and Roberts [2003], and lie in the range 1-200 ohm/m in the upper layers of the crust (σ=1-0.005 S/m). We choose a value of 0.01 S/m as being representative of this range (a great deal of the volume is in the upper conductivity range). For the profile, we follow Molchanov et al. [1993] who have assued an exponential profile similar to that show in Fig 3i.

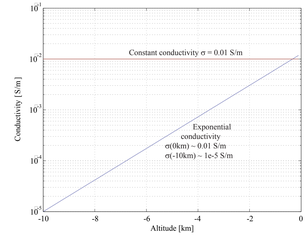

Figure 3i: Ground conductivity profile showing exponential and constant conductivity behaviour.

Summary:

- We have developed a full-wave code withh realistic medium parameters to model the wave propagation from below the Earth's surface to the topside ionosphere.
- Results indicate that the lower frequencies are able to penetrate the ionosphere with only moderate attenuation, and below ~10 Hz, both penetrating (RH) and non-penetrating (LH) modes can traverse the ionosphere.
- In the ground portion of the propagation, it was found the attenuation increased with frequency but that below a certain value, reflection from the interface dominated wave power.